Spectral simulations of tidal flows in weakly deformed spheres

Jérémie Vidal, David Cébron

Spectral simulations of tidal flows in weakly deformed spheres

Jérémie Vidal[1] & David Cébron[1]

[1] Université Grenoble Alpes, CNRS, ISTerre, Grenoble, France
jeremie.vidal@univ-grenoble-alpes.fr

Résumé. Due à la présence de compagnons orbitaux, les planètes et étoiles sont généralement soumises à des forçages orbitaux harmoniques, comme les marées ou la précession. Ces forçages déforment les enveloppes fluides en ellipsoïdes et peuvent générer des instabilités, comme l'instabilité elliptique. Dans le régime non linéaire, ces instabilités peuvent entretenir une turbulence d'ondes et générer des champs magnétiques dynamos. Cependant, elles ont été étudiées (numériquement et expérimentalement) uniquement pour des paramètres physiques très éloignés des valeurs géophysiques et astrophysiques. Nous proposons une nouvelle approche numérique, valide dans la limite des faibles déformations et des faibles diffusions. Nous avons implémenté cette méthode dans deux codes numériques spectraux, linéaires et non linéaires. Nous reportons les premiers résultats obtenus pour le forçage de marée, que nous comparons aux résultats de la littérature. Cette approche permet d'envisager l'avenir de faire des simulations numériques directes plus réalistes des écoulements générés par les forçages orbitaux en géométrie faiblement déformée.

Abstract. Celestial fluid bodies (e.g. planets, stars), orbited by gravitational companions, undergo harmonic orbital forcings, such as tides or precession. These orbital forcings deform fluid bodies into ellipsoids and generate fluid instabilities, e.g. the elliptical instability. The nonlinear outcome of these instabilities can sustain a wave turbulence regime and drive self-sustained, dynamo magnetic fields. However, orbitally driven instabilities have only been studied in the achievable range of parameters (i.e. large deformations and overestimated diffusive effects) that is far from the expected regime in geo and astrophysics. We advocate the use of an alternative numerical method to simulate fluid instabilities (i) in weakly deformed non-axisymmetric domains and (ii) in the weak diffusive regime. We have implemented this method within two spectral codes, devoted to linear and nonlinear computations. We report preliminary results benchmarked against the tidal forcing. This method paves the way for more realistic numerical simulations of orbitally driven flows in weakly deformed fluid containers.

1 Introduction

Celestial fluid bodies often undergo orbital (i.e. tidal) harmonic forcings (e.g. tides, precession, libration), due to the presence of orbital companions. These forcings deform fluid bodies into ellipsoids at first order. The ellipsoidal deformation generates a pressure torque at the fluid boundary, which overcomes the viscous coupling in the limit of vanishing viscosity in geo and astrophysics. This strongly affects the dynamics of fluid layers. Orbital forcing could also sustain dynamo magnetic fields, as confirmed by proof-of-concept numerical simulations [3,24,17]. However, numerical simulations of flows in deformed fluid containers are difficult to carry out. Indeed, spherical containers are much easier to handle numerically than non-spherical ones. Thus, numerical codes based on local methods, that can handled deformed geometries, have been used. Finite-volume codes have been developed [4,21], as well as finite-element codes in spheroidal geometry [25,26]. However, the latter authors considered only stress-free boundary conditions, which can lead to difficulties with angular momentum conservation and to spurious behaviours in axisymmetric geometries [9]. Simulations have also been carried out by using the Nek5000 code [6], based on the spectral element method. Pseudo-spectral codes, relying on spectral Galerkin expansions in certain directions, may be of interest. Indeed, local codes are generally less efficient than spectral codes, that benefit from (i) the spectral convergence and (ii) a fast spectral transform to (generally) perform simulations with values of dimensionless numbers closer to the astrophysical values. A self-consistent spectral method should be based on ellipsoidal harmonics. Considering the effectiveness of spectral decompositions based on spherical

harmonics [18], we may naively expect to obtain a generalisation in ellipsoidal domains. Unfortunately, a straightforward extension is impossible [15]. Other spectral methods have been proposed [14,20,11], but none of them deal with non-axisymmetric deformed containers.

We aim at presenting an innovative method, that can be implemented in any spherical spectral code, to study the dynamics of orbitally driven flows in weakly deformed, non-axisymmetric rigid containers. The paper is divided as follows. In §2, we introduce the physical model we are interested in and then we present the foundations of our method than can be implemented in spherical geometry. Then in §3, we benchmark our method on a test case (the elliptical instability). Finally, §4 ends the paper with a conclusion and draws some research perspectives.

2 Formulation of the problem

2.1 Mathematical modelling

We describe an idealised model of orbitally driven flows, suitable for fluid mechanics' studies, that mimics the astrophysical problem. We consider a Newtonian, incompressible fluid of homogeneous density ρ_* and uniform kinematic viscosity ν. The fluid is enclosed within a triaxial ellipsoidal container, rotating with the angular velocity $\boldsymbol{\Omega}(t)$ in the inertial frame. Ellipsoidal semi-axes (a, b, c) are steady in the frame rotating with $\boldsymbol{\Omega}(t)$, defined in the following as the body frame. In this frame, the ellipsoidal boundary is given by $(x/a)^2 + (y/b)^2 + (z/c)^2 = 1$. We denote $\beta_0 = |a^2 - b^2|/(a^2 + b^2) \geq 0$ the equatorial ellipticity and Ω_s the typical fluid angular velocity. We choose a typical length R_* as length scale, Ω_s^{-1} as time scale and $R_*\Omega_s$ as velocity scale. For the sake of concision, the dimensionless variables are noted as their dimensional counterparts. The dimensionless, incompressible, governing equations for the velocity field $\boldsymbol{v}$ are in the body frame

$$\frac{\partial \boldsymbol{v}}{\partial t} + (\boldsymbol{v}\cdot\boldsymbol{\nabla})\boldsymbol{v} + 2\,\boldsymbol{\Omega}(t)\times\boldsymbol{v} = -\nabla P + Ek\,\nabla^2\boldsymbol{v} + \boldsymbol{r}\times\frac{\mathrm{d}\boldsymbol{\Omega}}{\mathrm{d}t}, \quad \boldsymbol{\nabla}\cdot\boldsymbol{v} = 0, \quad \boldsymbol{v}\cdot\boldsymbol{n} = 0, \tag{1}$$

where $\boldsymbol{n}$ is the unit outward vector normal to the ellipsoidal boundary, P a dimensionless reduced pressure term and $Ek = \nu/(\Omega_s R_*^2)$ the Ekman number (based on the fluid angular velocity). Equations (1) contain the idealised physics to model the hydrodynamics of orbitally driven flows. They can be completed to take into account buoyancy effects and magnetic fields if necessary [24].

2.2 The new method

We propose an innovative method, inspired by astrophysical studies [5], to solve equations (1) in weakly deformed spherical containers. We assume that the fluid domain is subjected to a tidal potential, expressed in the inertial frame by the gravitational potential Ψ_t. The latter potential is proportional to solid spherical harmonics $r^l Y_l^m(\theta,\varphi)$, in which (r,θ,φ) are the spherical coordinates centred on the centre-of-mass of the fluid body and $Y_l^m(\theta,\varphi)$ is the spherical harmonic of degree l and azimuthal order $-l \leq m \leq l$. Note that the fluid boundary is exactly ellipsoidal if the tidal potential is any linear combination of tidal components of degree $l = 2$. Then, we assume that the fluid is enclosed within a spherical domain that mimics a stellar or planetary envelope. Thus, the tidal potential drives a radial flow at the boundary, i.e. $\boldsymbol{v}\cdot\boldsymbol{n} = F(\Psi_t)$ where F is a known function [16]. This radial flow is an inhomogeneous boundary condition, that is asymptotically valid in the limit of small deformations (e.g. $\beta_0 \ll 1$) and vanishing viscosities ($Ek \to 0$).

Full equations (1) can be solved by converting the influx from the radial flow into a body force, see p.76 of [8]. We determine a particular potential 'non-wavelike' solution $\boldsymbol{v}_p$, having the properties

$$\boldsymbol{\nabla}\cdot\boldsymbol{v}_p = 0, \quad \boldsymbol{\nabla}\times\boldsymbol{v}_p = \boldsymbol{0} \quad \text{and} \quad \boldsymbol{v}_p\cdot\boldsymbol{n} = F(\Psi_t). \tag{2}$$

Then, by setting $\boldsymbol{v} = \boldsymbol{v}_p + \widetilde{\boldsymbol{v}}$, the 'wavelike' flow $\widetilde{\boldsymbol{v}}$ is solution of equations (1) by adding a body force in the right-hand side. This decomposition is known as the the non-wavelike/wavelike decomposition in

astrophysics [16]. This method has been validated to compute (linear and nonlinear) tidally forced waves of small wavelength [16,5]. The method is *a priori* not directly suited to seek the leading order, forced response of the fluid cavity to the orbital forcing. Indeed, this forced flow is a physically large-scale flow $\boldsymbol{U}$, which is sensitive to the boundary shape. However, in the particular case of the tidal component $\Psi_t \propto r^2 Y_2^0$, associated with an orbital companion moving around the host fluid body on a circular orbit, the particular (dimensionless) flow $\boldsymbol{v}_p$ reduces to

$$\boldsymbol{U}(\boldsymbol{r}) = (1-\Omega_0)\left[-(1+\beta_0)\, y\, \widehat{\boldsymbol{x}} + (1-\beta_0)\, x\, \widehat{\boldsymbol{y}}\right], \tag{3}$$

with $\boldsymbol{r} = (x, y, z)^T$ the position vector in the body frame and $(\widehat{\boldsymbol{x}}, \widehat{\boldsymbol{y}}, \widehat{\boldsymbol{z}})$ the unit Cartesian vectors. It turns out that this is the exact ellipsoidal basic flow in ellipsoids, solution of equations (1) with the orbital angular velocity $\boldsymbol{\Omega} = (0, 0, \Omega_0)^T$.

The above discussion suggests that we can split the total velocity field $\boldsymbol{v}$ as a basic flow $\boldsymbol{U}$, that is an exact solution of equations (1) in a deformed (e.g. ellipsoidal) fluid domain, and a perturbation $\boldsymbol{u}$, solution of the nonlinear equations in a spherical domain

$$\frac{\partial \boldsymbol{u}}{\partial t} + (\boldsymbol{u}\cdot\boldsymbol{\nabla})\boldsymbol{u} + 2\,\boldsymbol{\Omega}(t)\times\boldsymbol{u} = -\nabla p + Ek\,\nabla^2\boldsymbol{u} - (\boldsymbol{u}\cdot\boldsymbol{\nabla})\boldsymbol{U} - (\boldsymbol{U}\cdot\boldsymbol{\nabla})\boldsymbol{u}, \quad \boldsymbol{\nabla}\cdot\boldsymbol{u} = 0, \tag{4}$$

where p is the reduced pressure. This assumption should be valid in the limit of (i) small deformations (e.g. $\beta_0 \ll 1$), such that the deformed fluid domain tends to a sphere, and (ii) vanishing viscosities ($Ek \to 0$), such that perturbations of high spatial complexity (i.e. of small wavelength, that are barely sensitive to the fluid boundary) are triggered. Then, equations (1) are supplemented by viscous stress-free conditions at spherical boundaries

$$\boldsymbol{u}\cdot\boldsymbol{n} = 0, \quad \boldsymbol{n}\times\left[\boldsymbol{n}\cdot\left(\boldsymbol{\nabla}\boldsymbol{u} + (\boldsymbol{\nabla}\boldsymbol{u})^T\right)\right] = \boldsymbol{0}, \tag{5}$$

that are often assumed to be valid for the velocity field in astrophysics. We further impose a zero angular momentum condition for $\boldsymbol{u}$. Coupled with conditions (5), this is equivalent to fix a non-zero constant angular momentum and stress-free conditions on the total velocity field $\boldsymbol{U} + \boldsymbol{u}$. Thus, we assume that the angular momentum of the fluid is only carried on by the basic flow $\boldsymbol{U}$. In ellipsoids, only large-scale flows, that are linear in Cartesian space coordinates, have a non-zero angular momentum [10]. These flows are filtered out within our framework. However, this assumption is *a priori* justified because they are generally not the preferred unstable modes for geo and astrophysical parameters [1,22].

3 Test case: the elliptical instability

3.1 Linear, inviscid stability analysis

We investigate the linear, inviscid hydrodynamic stability of the tidal basic flow (3). This flow is prone to the elliptical instability [12], i.e. a nonlinear parametric instability coupling two inertial waves of the fluid with the basic 'elliptical' wave flow. The elliptical instability can be studied with a local stability analysis [22]. The largest inviscid growth rate σ can be obtained analytically in the limit $\beta_0 \ll 1$. It reads

$$\frac{\sigma}{|1-\Omega_0|} = \max_{\theta_0} \frac{1}{4}\sqrt{(1+\cos\theta_0)^4\,\beta_0^2 - 4\left[2 - 4\left(1+\widetilde{\Omega}_0\right)\cos\theta_0\right]^2}, \tag{6}$$

with $\widetilde{\Omega}_0 = \Omega_0/(1-\Omega_0)$ and $0 \le \theta_0 \le \pi$ an adjustable parameter chosen to maximise σ. In the asymptotic limit $\beta_0 \to 0$, the elliptical instability only exists in the allowable range $-1 \le \Omega_0 \le 3$. However, formula (6) shows that the elliptical instability is actually excited on a wider allowable range for finite values of β_0, as a result of geometric detuning effects (hidden in the optimisation over θ_0). The elliptical instability actually exists in the orbital range $(\beta_0+1)/(\beta_0-1) \le \Omega_0 \le 3$.

The emphasis is here to compare formula (6) with theoretical stability results obtained by assuming spherical perturbations. We have extended the SIREN code [22], to handle arbitrary spherical perturbations superimposed of the elliptical flow (3). We outline here the method [23,22]. The only (minor)

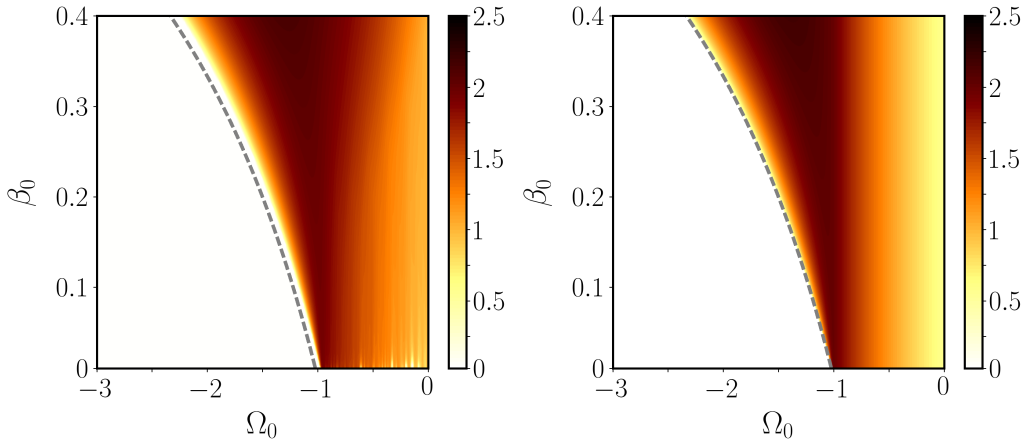

(a) Global analysis ($n = 10$) (b) Local formula (6)

Figure 1. Areas of instability of the tidal flow (3) in the (β_0, Ω_0) plane. Resolution in the parameter space is 200^2. Colour map shows σ/β_0. Ellipsoidal semi-axes $a = \sqrt{1+\beta_0}$, $b = \sqrt{1-\beta_0}$ in formula (3) and spherical perturbations ($a = b = c = 1$). Grey dashed line $\Omega_0 = (1 + \beta_0)/(1 - \beta_0)$ is the lower bound of the unstable zone. White areas are (marginally) stable areas.

modification is that we handle flow perturbations bounded within a container with a different ellipticity than the ellipticity of the 'basic' container, in which basic flow (3) is an exact solution of equations (1). We project the velocity perturbation onto an exact polynomial Galerkin basis, expressed in Cartesian coordinates $\{x, y, z\}$, of maximum degree n. This basis is made of polynomial elements $\{\boldsymbol{p}_i(\boldsymbol{r})\}$, which are divergenceless ($\boldsymbol{\nabla}\cdot\boldsymbol{p}_i = 0$) and satisfy the impermeability boundary condition ($\boldsymbol{p}_i\cdot\boldsymbol{n} = 0$) at the outer spherical boundary. For a given maximum degree n, the number of basis elements is $n(n+1)(2n+7)/6$ [22]. Then, we seek flow perturbations upon the tidally driven flow (3) as a linear combination of polynomial elements, i.e. $\boldsymbol{u} = \sum_i \alpha_i \boldsymbol{p}_i$ with $\{\alpha_i\}$ modal coefficients. This expansion leads to a generalised eigenvalue problem, that is solved by using standard numerical methods. We obtain the largest growth rate σ of the instability, that is a monotonic increasing function of n. Therefore, this method gives only sufficient conditions for instability for a given degree n, and the growth rate converges to its maximum value when $n \to \infty$.

We compare, in figure 1, formula (6) and our results computed with the modified SIREN code for the degree $n = 10$. We find that the two stability maps are globally in good agreement. First, instabilities in (a) exist only in areas in which they are expected from formula (6). Second, the largest growth rate of spherical perturbations in (a) is identical to the one obtained in (b), that is an upper bond for the inviscid growth rate of the elliptical instability in ellipsoids [22]. Then, one point is worthy of comment. We have shown only the orbital range $-3 \leq \Omega_0 \leq 0$, which is representative of the worst possible range for the validity of the method. Indeed, large-scale vigorous modes (e.g. spin-over modes $n = 1$) can be strongly excited in the range $-0.5 \leq \Omega_0 \leq 0$, even when $\beta_0 \ll 1$ [1,22]. This is no longer true outside of this range, in particular when $0 \leq \Omega_0 \leq 3$ [1,22]. We find that the growth rates are slightly increased (at most by a factor two) when $-0.5 \leq \Omega_0 \leq 0$, due to the presence of these large-scale (spherical) modes that are not modelled by the local analysis. However, outside of this range, the growth rates σ obtained by considering spherical perturbations are quantitatively in excellent agreement with local formula (6). Therefore, this comparison validates our method on the linear regime of the instability, at least in the physically relevant range of parameters.

3.2 Numerical simulations

We now benchmark the nonlinear regime of the elliptical instability, by using direct numerical simulations. Governing equations (4) are solved with the open source, parallel code XSHELLS [19,24]. It uses second

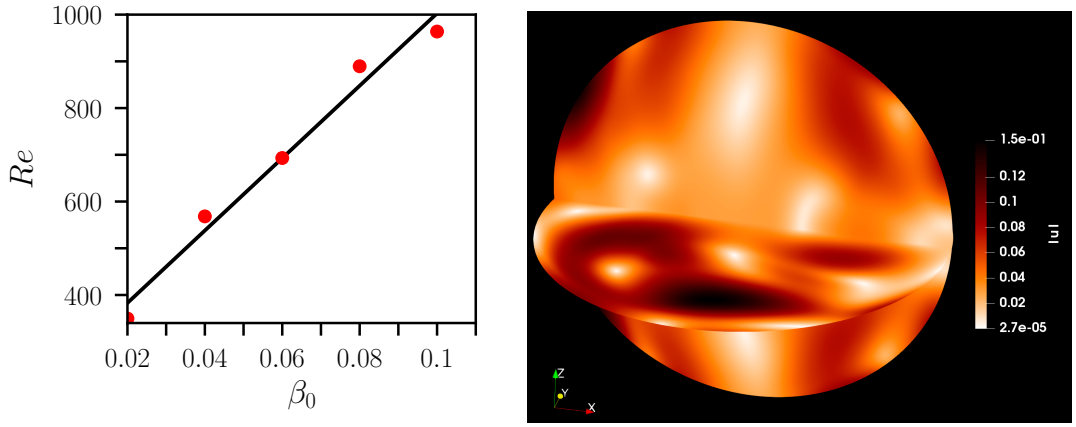

(a) (b)

Figure 2. Nonlinear simulations performed with the XSHELLS code. (a) Reynolds number Re as a function of the equatorial ellipticity β_0. Solid line is the scaling $Re \propto \beta_0$. (b) Three-dimensional snapshot of the velocity magntitude $|\boldsymbol{u}|$ in the fluid domain. $\beta_0 = 0.08$. The fluid rotation axis is along the Z axis.

order finite differences in radius and a spectral spherical harmonic expansion [18]. The time-stepping scheme is of second order in time, and treats the diffusive terms implicitly, while the nonlinear and Coriolis terms are handled explicitly. We have extended the XSHELLS code to handle arbitrary steady basic flows $\boldsymbol{U}(\boldsymbol{r})$. All simulations were performed at $\Omega_0 = 0$ and $Ek = 10^{-4}$, for several values of the equatorial ellipticity $\beta_0 \ll 1$. The spatial discretisation uses $N_r = 224$ radial points, $l_{\max} = 128$ spherical harmonic degrees and $m_{\max} = 64$ azimuthal wave numbers. We made sure that our simulations are numerically converged by varying the spatial resolution.

To quantify the nonlinear outcome of the instability, we compute the kinetic energies

$$E(\boldsymbol{u}) = \int_V \frac{|\boldsymbol{u}|^2}{2}\,\mathrm{d}V \quad \text{and} \quad E(\boldsymbol{U}) = \int_V \frac{|\boldsymbol{U}|^2}{2}\,\mathrm{d}V, \tag{7}$$

with $V = 4\pi/3$ the dimensionless volume of the sphere. Then, we compute the Reynolds number of the nonlinear flow $\boldsymbol{u}$ as $Re = Ro/Ek$, with $Ro = \sqrt{E(\boldsymbol{u})/E(\boldsymbol{U})}$ the Rossby number. In figure 2 (a) we show that the evolution of Re as β_0 varies. The nonlinear regime of the instability is well captured in our simulations. Indeed, Re scales as β_0 [7] and the saturated energy level is in good agreement with published global simulations [24], yielding $Re/\beta_0 \sim 10^4$. Saturated flows, that are symmetric with respect to the equatorial plane, can be predominantly columnar (i.e. aligned with and almost invariant along the axis of rotation) [2] or three-dimensional, possibly due to nonlinearly interacting waves [13]. The latter nonlinear regime is illustrated in figure 2 (b).

4 Conclusion and perspectives

We have proposed a new method to perform spectral simulations of orbitally (i.e. tidally) driven flows in weakly deformed spherical containers, that are idealised models of celestial fluid bodies subjected to harmonic orbital forcings. We have implemented this method within two available codes, namely the (linear) stability code SIREN [22] and the (nonlinear) spherical code XSHELLS [19,24]. To benchmark our approach, we have considered tidal flows and obtained a quite good agreement with previously published results. These preliminary results pave the way for more realistic future numerical simulations, as outlined in figure 3. On one hand, DNS in true ellipsoids are limited to moderate values $Ek \geq 10^{-5}$ and $\beta_0 \geq 10^{-2}$ [6,7,17]. On the other hand, DNS performed with the XSHELLS code can use Ekman numbers as small as $Ek = 10^{-7}$ [19], that are closer to the expected values of celestial fluid bodies. Therefore, smaller

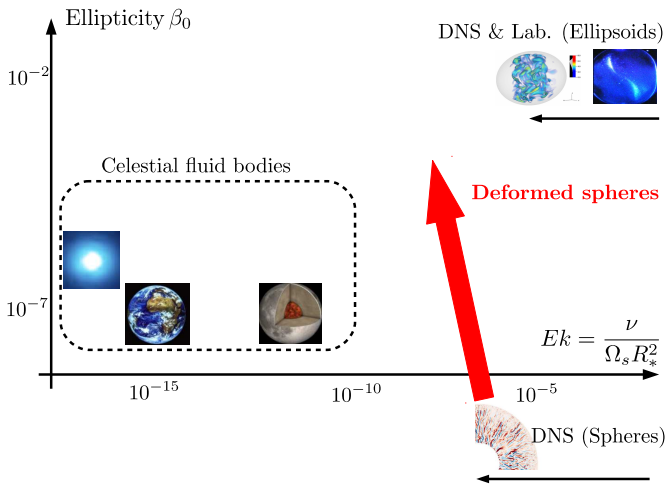

Figure 3. Typical values of the Ekman number Ek and of the equatorial ellipticity $\beta_0 = |a^2 - b^2|/|a^2 + b^2|$ of direct numerical simulations (DNS), laboratory experiments and celestial fluid bodies. Laboratory experiments and DNS usng local methods in ellipsoids are limited to moderate values of Ek, typically $Ek \geq 10^{-5}$. Because of this overestimated diffusion, the fluid boundary must be over-deformed to have a pressure torque that overcomes the viscous torque. DNS using spherical codes but mimicking weakly deformed containers can alleviate this problem to reach smaller values of Ek and β_0 (red arrow).

values of Ek (and so of β_0) than the ones we have used in this paper ($\beta_0 \geq 2 \times 10^{-2}$, $Ek = 10^{-4}$) are within reach. We will carry out new simulations in a more physically relevant range of parameters in a near future.

References

1. Barker, A. J, Braviner, H. J. & Ogilvie, G. I. 2016 *MNRAS* **459** (1), 924–938.
2. Barker, A. J. & Lithwick, Y. 2013 *MNRAS* **435** (4), 3614–3626.
3. Cébron, D. & Hollerbach, R. 2014 *ApJ* **789** (1), L25.
4. Ernst-Hullermann, J., Harder, H. & Hansen, U. *Geophys. J. Int.* **195** (3), 1395–1405.
5. Favier, B., Barker, A. J., Baruteau, C. & Ogilvie, G. I. 2014 *MNRAS* **439** (1), 845–860.
6. Favier, B., Grannan, A. M., Le Bars, M. & Aurnou, J. M. 2015 *Phys. of Fluids* **27** (6), 066601.
7. Grannan, A. M., Favier, B., Le Bars, M. & Aurnou, J. M. 2017 *Geophys. J. Int.* **208** (3), 1690.
8. Greenspan, H. P. 1968 *The theory of Rotating Fluids*
9. Guermond, J.-L., Léorat, J., Luddens, F. & Nore, C. 2013 *Eur. J. Mech. B Fluid* **39**, 1–10.
10. Ivers, D. J. 2017a *GAFD* **111** (5), 333–354.
11. Ivers, D. J. 2017b *GAFD* **473** (2206), 20170432.
12. Kerswell, R. R. 2002 *ARFM* **34** (1), 83–113.
13. Le Reun, T., Favier, B., Barker, A. J. & Le Bars, M. 2017 *Phys. Rev. Let.* **119** (3), 034502.
14. Lorenzani, S. & Tilgner, A. 2001 *J. Fluid Mech.* **447**, 111–128.
15. Morse, P. M. & Feshbach, H. 1953 *Methods of Theoretical Physics*
16. Ogilvie, G. I. 2014 *ARAA* **52**, 171–210.
17. Reddy, K. S., Favier, B. & Le Bars, M. 2018 *Geophys. Res. Lett. (in press)* .
18. Schaeffer, N. 2013 *Geochemistry, Geophysics, Geosystems* **14** (3), 751–758.
19. Schaeffer, N., Jault, D., Nataf, H.-C. & Fournier, A. 2017 *Geophys. J. Int.* **211** (1), 1–29.
20. Schmitt, D. & Jault, D. 2004 *J. of Comp. Phys.* **197** (2), 671–685.
21. Vantieghem, S., Sheyko, A. & Jackson, A. 2016 *Geophys. J. Int.* **204** (2), 1376–1395.
22. Vidal, J. & Cébron, D. 2017 *J. Fluid Mech.* **833**, 469–511.
23. Vidal, J., Cébron, D. & Schaeffer, N. 2016 *Comptes-Rendus 19e RNL* p. 121.
24. Vidal, J., Cébron, D., Schaeffer, N. & Hollerbach, R. 2018 *MNRAS*.
25. Wu, C.-C. & Roberts, P. H. 2009 *GAFD* **103** (6), 467–501.
26. Wu, C.-C. & Roberts, P. H. 2013 *GAFD* **107** (1-2), 20–44.